# Electronic Supplementary Information (ESI)

# Intramolecular Exciplex Featuring a bis-sp$^3$ C-Locked Acceptor-Donor-Acceptor Sandwich

Feng-Ming Xie, Han-Yang Wang, Hao-Ze Li, Kai Zhang, Yang Shen, Jianhua Zou, Yan-Qing Li,* Jian-Xin Tang*

[*] Dr. F.-M. Xie, H.-Y. Wang, Dr. Y. Shen, Prof. J.-X. Tang
Jiangsu Key Laboratory for Carbon-Based Functional Materials & Devices
Institute of Functional Nano & Soft Materials (FUNSOM), Soochow University
Suzhou, Jiangsu 215123 (P. R. China)
E-mail: jxtang@suda.edu.cn (J.-X. Tang)

H.-Z. Li, Prof. Y.-Q. Li
School of Physics and Electronic Science
East China Normal University
Shanghai 200062 (P. R. China)
E-mail: yqli@phy.ecnu.edu.cn (Y.-Q. Li)

K. Zhang, Prof. J. X. Tang
Macao Institute of Materials Science and Engineering (MIMSE)
Faculty of Innovation Engineering
Macau University of Science and Technology
Taipa, Macau 999078 (P. R. China)
E-mail: jxtang@must.edu.mo (J.-X. Tang)

Dr. J. Zou
Guangzhou New Vision Opto-Electronic Technology Co., Ltd.
Guangzhou, Guangdong 510730 (P. R. China)

## Table of Contents

## Synthesis and characterization

**Table S1**. List of raw material information.

| Drug name | Drug purity | Drug manufacturers |
|---|---|---|
| 1,4-dibromo-2,5-difluorobenzene | 98.0% | Bidepharm |
| Phenoxazine | 98.0% | Aladdin |
| 2,4-Diphenyl-6-(4-(4,4,5,5-tetramethyl-1,3,2-dioxaborolan-2-yl)phenyl)-1,3,5-triazine | 99.0% | Aladdin |
| 2-Bromo-9-fluorenone | 98.0% | Alpha |
| Tetrahydrofuran Anhydrous (stabilized with BHT) | 99.0% | TCI |
| 1,4-Dioxane | 99.0% | Enox |
| Tert-Butyllithium solution | 1.3 M in Pentane | Aladdin |
| Potassium carbonate | 99.0% | Alpha |
| Tetrakis(triphenylphosphine)palladium(0) | 99.0% | J&K |
| Hydrochloric acid | 36.0% | Enox |
| Acetic Acid | 99.0% | Enox |

*Chemical Synthesis:* All the reagents purchased from commercial sources were used without further purification. All the reactions were performed under nitrogen atmosphere, and the crude products were purified by column chromatography before characterizations and device fabrication.

*Measurements and Characterization:* The chemical structures were determined by $^{1}H$ and $^{13}C$ nuclear magnetic resonance (NMR) spectra with Bruker AVANCE III type NMR Spectrometer in $CDCl_3$ solution, Matrix-assisted laser desorption/ionization time-of-flight (MALDI-TOF) mass spectrometer, Elemental analysis test using Vario Micro cube elemental analyzer. and single-crystal X-ray diffraction. Ultraviolet–visible

(UV-Vis) absorption and photoluminescence (PL) spectra were recorded at room temperature with a Perkin-Elmer Lambda 750 UV-Vis spectrophotometer and a FM-4 type fluorescence spectrophotometer (JY company, French), respectively. The optical bandgap ($E_g$) was determined from the onset of the absorption spectra. Low-temperature phosphorescence spectra were measured with a FLS 920 spectrometer (Einburgh Corporation) in neat film at 77 K. The absolute photoluminescence quantum yields (PLQYs) of the doped and non-doped films were obtained with a C9920-02G type fluorescence spectrophotometer (HAMAMASTU, Japan) with an integrating sphere at room temperature under nitrogen atmosphere. Transient PL decay spectra were measured with a Quantaurus-Tau fluorescence lifetime spectrometer (C11367-03, Hamamatsu Photonics) with a pulse wavelength of 373 nm, pulse width of 100 ps. The prompt and delayed PL spectra were measured by using a streak camera system (Hamamatsu Photonics, C4334) equipped with a cryostat and an excitation wavelength of 373 nm under a vacuum.

*Theoretical Calculations*: All the quantum chemical calculations were performed using a DFT method in Gaussian 09 program package. The ground-state geometries were optimized by using a TD-DFT approach at the B3LYP/6-311G(d,p) level. The singlet and triplet excited-state properties were calculated according to the optimized geometries.

*Cyclic voltammetry measurements:*The HOMO and LUMO levels were determined from the Cyclic voltammetry (CV) measurements. CV measurements were conducted on a RST 3100 electrochemical analysis equipment at room temperature with a

conventional three electrode configuration, consisting of a platinum disk working electrode, a platinum wire counter electrode, a Ag/AgCl reference electrode, and the supporting electrolyte of tetrabutylammonium hexafluorophosphate (0.1 M). The cyclic voltammograms were obtained at a scanning rate of 50 mV $s^{-1}$ with DCM solution.

*Thermal properties:* Thermal gravimetric analysis (TGA) was carried out with an HCT-2 instrument at a heating rate of 10 °C $min^{-1}$ under nitrogen atmosphere.

*Device Fabrication and Measurements*: OLEDs were fabricated on the patterned indium-tin-oxide (ITO)-coated glass substrates with a sheet resistance of ~15 Ω per square. The ITO-coated glass substrates were successively cleaned in an ultrasonic bath with acetone, ethanol, and deionized water, and then dried in an oven at 110 °C. After the UV-ozone treatment for 15 minutes, the ITO-coated glass substrates were transferred into a high-vacuum deposition chamber (base pressure ≤ $2\times10^{-6}$ mbar) for the thermal deposition of organic materials and metal electrodes through a shadow mask. After the film depositions, the fabricated devices were transferred to the nitrogen-filled glovebox for the encapsulation with a glass cap and epoxy glue. Current density-voltage-luminance (J-V-L) characteristics and EL spectra of the devices were measured simultaneously with a source meter (Keithley model 2400) and a luminance meter/spectrometer (PhotoResearch PR670). The CIE 1931 colour coordinates were obtained from the EL spectra.

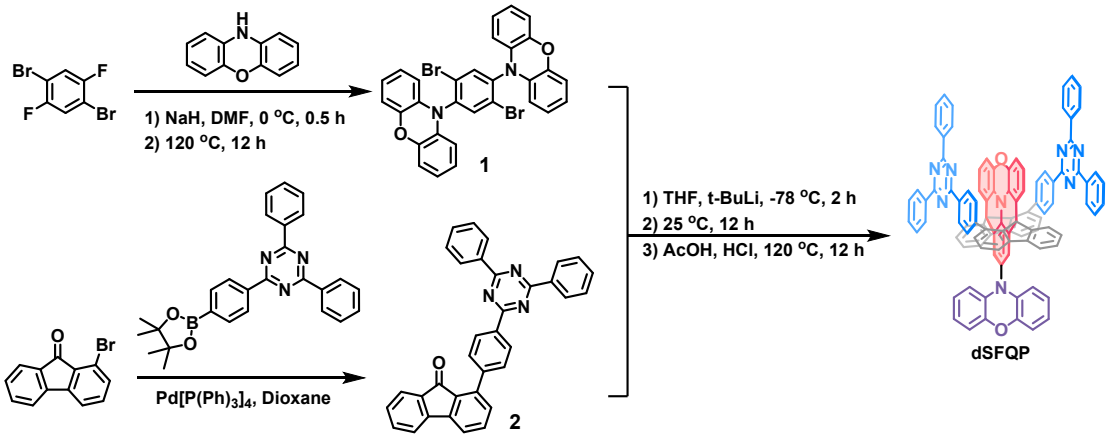


**Scheme S1**. The synthetic route of **dSFQP**.

**Synthesis of 10,10'-(2,5-dibromo-1,4-phenylene)bis(10H-phenoxazine) (1):**

A mixture of 10H-phenoxazine (3.37 g, 18.45 mmol) and NaH (0.88 g, 37.90 mmol) were stirred for 30 min in DMF (40 mL) in three-neck bottle under nitrogen at 0 ℃. Then the 1,4-dibromo-2,5-difluorobenzene (2.00 g, 7.38 mmol) was injected into the bottle and the reaction mixture was heated up to 120 ℃ and reacted for 24 h. After cooled down to room temperature, filtered and the solid washed with n-Hexane (n-H). The solid was purified by column chromatography on silica gel eluted with (dichloromethane/n-H, 1:4) to give the **1** (4.12 g, 6.87 mmol, yield: 87%). $^1$H NMR (400 MHz, $CDCl_3$) δ 7.84 (s, 2H), 6.87 – 6.70 (m, 12H), 6.21 – 6.02 (m, 2H), 5.91 (ddd, $J$ = 14.5, 6.9, 1.6 Hz, 2H). MALDI-TOF-MS (m/z) of $C_{30}H_{18}Br_2N_2O_2$ for [M]+: calcd. 597.97; found, 598.606.

**Synthesis of 2-(4-(4,6-diphenyl-1,3,5-triazin-2-yl)phenyl)-9H-fluoren-9-one (2):**

A mixture of 1-bromo-9-fluorenone (1.50 g, 3.45 mmol), 2,4-diphenyl-6-(4-(4,4,5,5-tetramethyl-1,3,2-dioxaborolan-2-yl)phenyl)-1,3,5-triazine (1.65 g, 3.80 mmol), $Pd(PPh_3)_4$ (0.07 g, 0.06 mmol), and $K_2CO_3$ (1.26 g, 9.11 mmol) were added in 150 mL

three-neck bottle under nitrogen. Then, a mixed solvent system of 1,4-dioxane and $H_2O$ (v/v =10:1) were injected into the bottle, and the reaction mixture was refluxed for 24 h. After cooling to room temperature, the mixture was poured into the water and extracted for twice with dichloromethane, and then the combined organic layers were evacuated to dryness and the resulting product was purified by column chromatography on silica gel with (dichloromethane/n-H, 1:1) to afford **2** (2.98 g, 6.12 mmol, yield: 91%).

**Synthesis of (9R,12'R)-1,1''-bis(4-(4,6-diphenyl-1,3,5-triazin-2-yl)phenyl)-10'-(10H-phenoxazin-10-yl)dispiro[fluorene-9,8'-benzo[9,1]quinolizino[3,4,5,6,7-klmn]phenoxazine-12',9''-fluorene] (dSFQP):**

In a nitrogen glove box, compound **1** (2.00 g, 3.42 mmol) was dissolved in 30 mL of dry tetrahydrofuran in a 250 mL reaction flask. The reaction flask was transferred to a low-temperature reactor, and after the temperature was stabilized at -78 °C, 1 M *t*-butyl lithium (13.50 mL, 13.50 mmol) was slowly added dropwise by a syringe. The resulting mixture was stirred at -78 °C for 2 hours, and then a tetrahydrofuran solution (30 mL) containing compound **2** (4.04 g, 8.50 mmol) was added over 30 minutes. The mixture was stirred overnight at room temperature. 10 mL of anhydrous ethanol was added to the mixture to stop the reaction, and the solvent was evaporated. The obtained solid was removed in 200 mL of dichloromethane and washed with 50 mL of anhydrous ethanol three times. The obtained trustworthiness can be directly used in the next step without further purification. The crude product was dissolved in 30 mL acetic acid, heated to

130 °C stirred for 30 min, and added with 8 mL hydrochloric acid (36%). After stirring and relaxing for 24 hours, the reaction solution was washed with ice water, extracted, and washed with n-hexane. The obtained solid was further purified by column chromatography using (dichloromethane/n-H, 1:4) as eluent, and got the product **dSFQP** (0.42 g, 0.31 mmol, yield: 18%). $^{1}$H NMR (400 MHz, $CDCl_3$) δ 8.88 – 8.61 (m, 12H), 8.61 – 8.47 (m, 4H), 8.12 (d, *J* = 7.9 Hz, 2H), 7.88 (t, *J* = 8.3 Hz, 2H), 7.75 (d, *J* = 7.6 Hz, 2H), 7.71 – 7.61 (m, 10H), 7.59 – 7.54 (m, 8H), 7.43 – 7.39 (m, 6H), 7.32 (d, *J* = 7.7 Hz, 2H), 7.27 – 7.11 (m, 4H), 6.87 – 6.64 (m, 4H), 6.53 (d, *J* = 8.1 Hz, 2H). $^{13}$C NMR (101 MHz, $CDCl_3$) δ 171.42, 171.42, 171.21, 171.13, 145.26, 143.35, 141.92, 140.14, 139.57, 136.40, 136.33, 136.20, 135.96, 134.80, 132.43, 132.38, 132.26, 129.02, 128.96, 128.91, 128.84, 128.71, 128.59, 128.54, 128.43, 128.38, 128.14, 128.00, 127.85, 127.68, 127.28, 127.20, 124.94, 122.86, 120.65, 119.94, 119.90, 119.28, 114.82, 112.57, 53.12, 53.03. MALDI-TOF-MS (m/z) of $C_{98}H_{58}N_8O_2$ for [M]+: calcd. 1378.471; found, 1378.886. Elemental analysis calcd. for $C_{98}H_{58}N_8O_2$: C, 85.32; H, 4.24; N, 8.12; found: C 85.01, H 4.20, N 7.98.

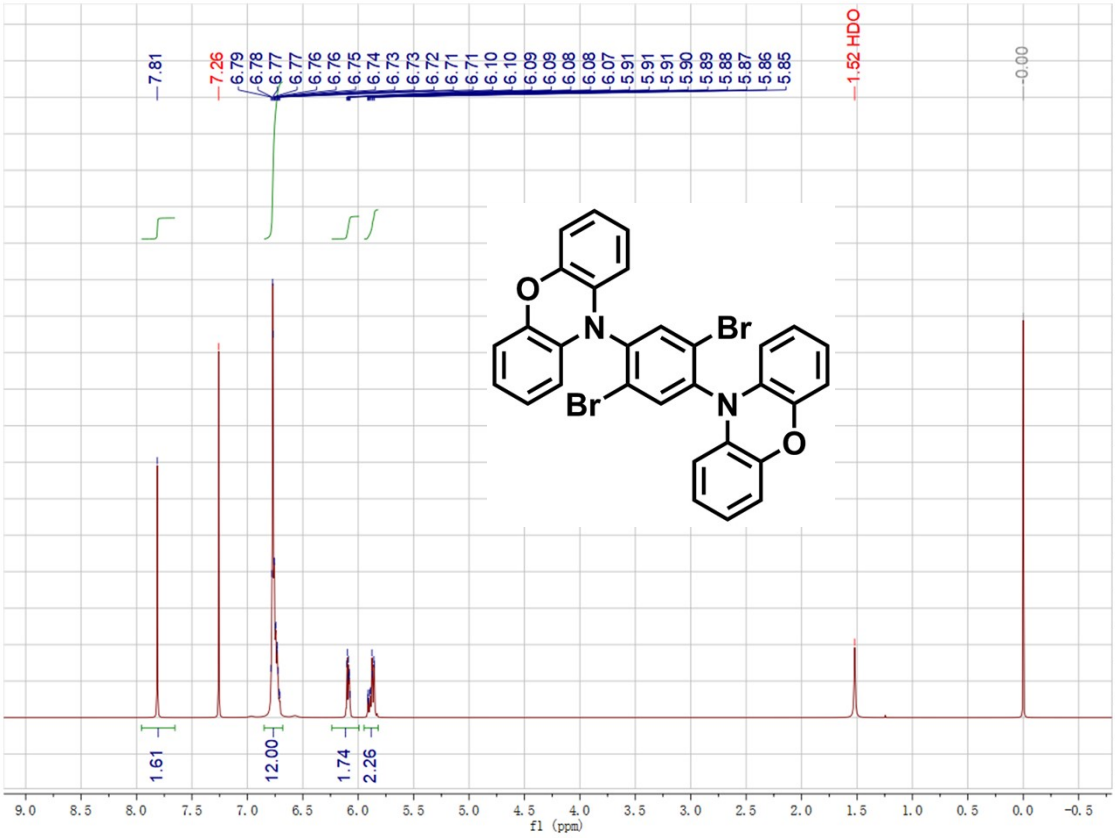


**Figure S1**. $^{1}$H NMR spectrum of compound **1**.

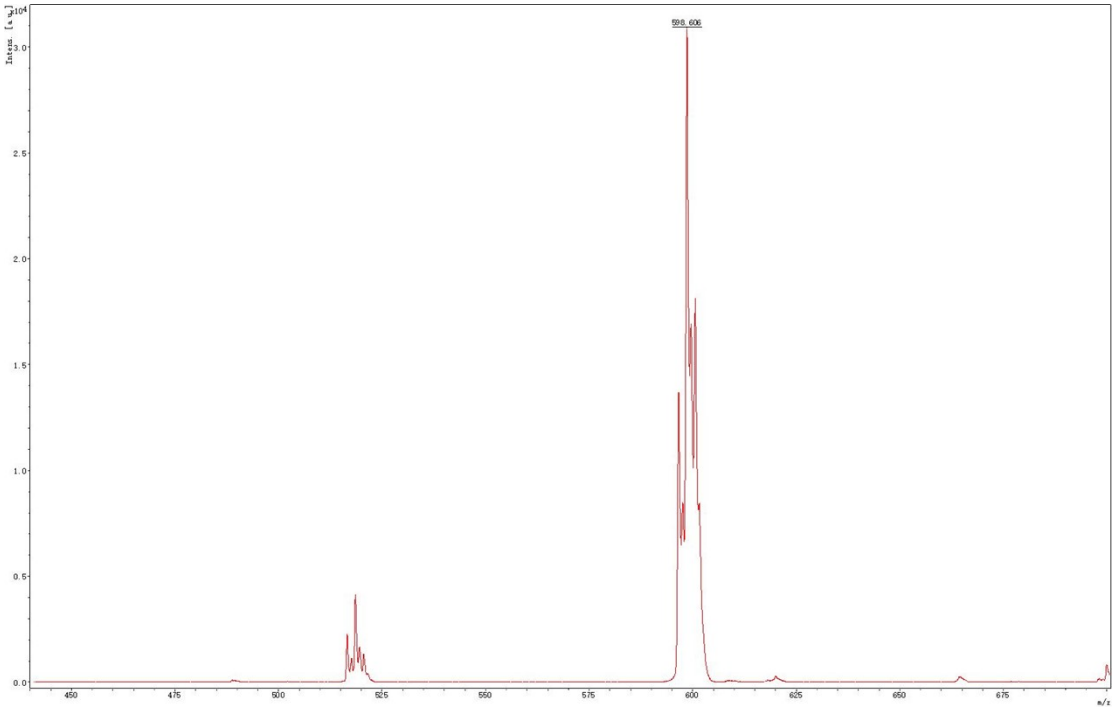


**Figure S2**. MALDI-TOF MS spectrum of compound **1**.

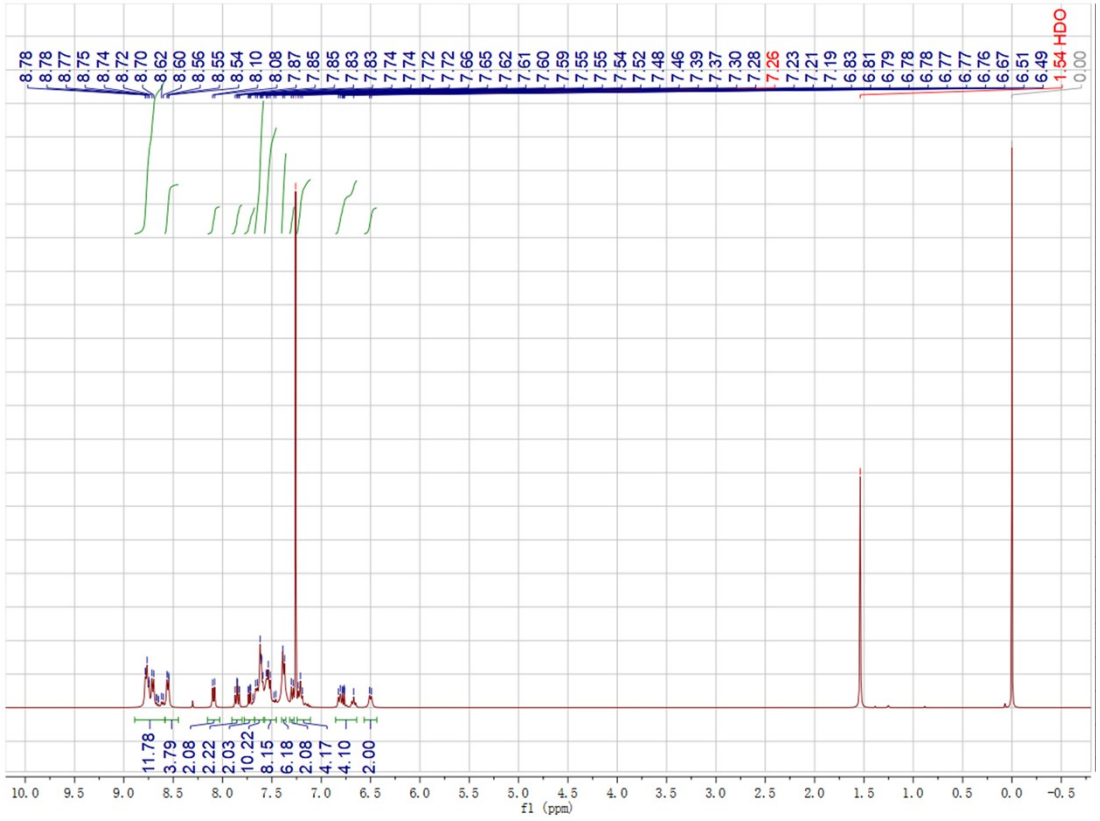


**Figure S3**. $^{1}$H NMR spectrum of **dSFQP**.

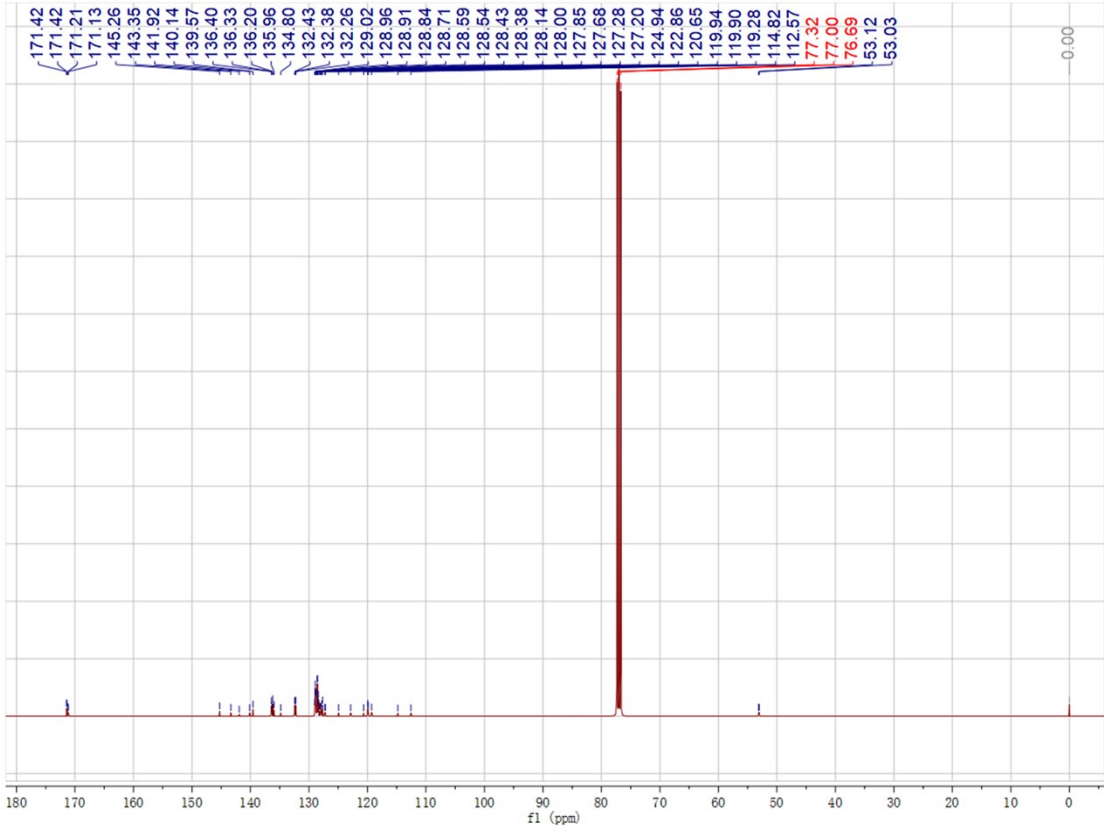


**Figure S4**. $^{13}C$ NMR spectrum of **dSFQP**.

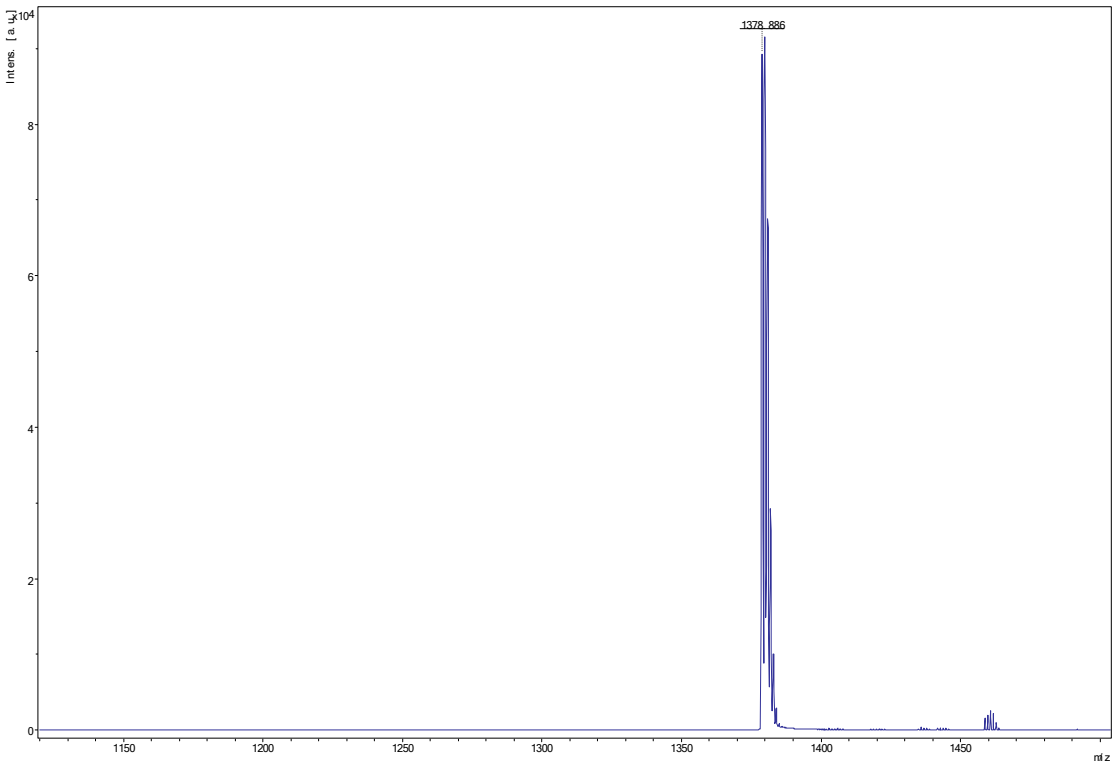


**Figure S5**. MALDI-TOF MS spectrum of **dSFQP**.

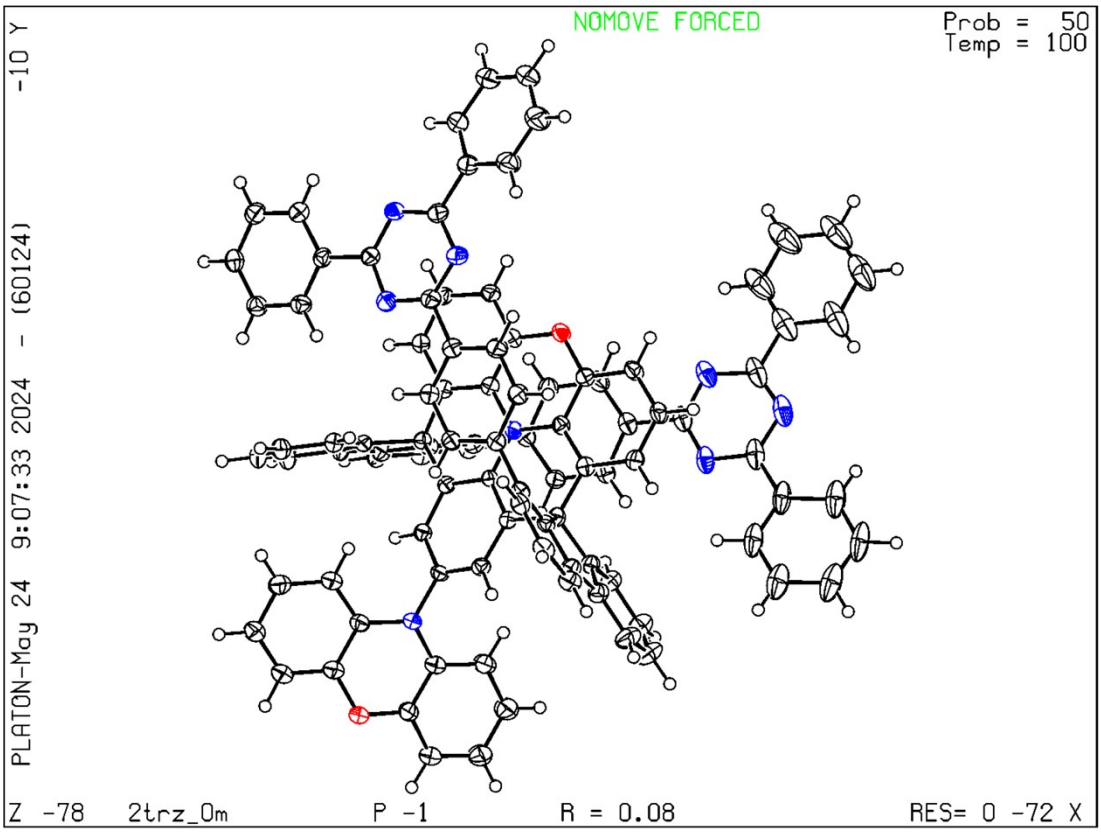


**Figure S6**. Ellipsoid plot of **dSFQP** obtained by single crystal diffraction.

**Table S2**. Crystal data and structure refinement for **dSFQP**. (CCDC number: 2294792)

| | |
|---|---|
| $2(C_{98}H_{58}N_8O_2)\cdot 2[CH_2Cl_2]\cdot 1[C_2H_6O]\cdot 2[CH_2Cl_2]$ | $Z = 1$ |
| $M_r = 3150.79$ | $F(000) = 1624.052$ |
| Triclinic, $P\bar{1}$ | $D_x = 1.356$ Mg m$^{-3}$ |
| $a = 14.2142$ (8) Å | Mo $K\alpha$ radiation, $\lambda = 0.71073$ Å |
| $b = 14.3406$ (7) Å | Cell parameters from 9933 reflections |
| $c = 19.3048$ (9) Å | $\theta = 2.2–26.4°$ |
| $\alpha = 97.833$ (2)° | $\mu = 0.22$ mm$^{-1}$ |
| $\beta = 93.512$ (2)° | $T = 100$ K |
| $\gamma = 99.176$ (2)° | Block, yellow |
| $V = 3834.6$ (3) Å$^3$ | 0.09 × 0.05 × 0.04 mm |
| *Bruker D8 VENTURE diffractometer* | 11025 reflections with $I$ ³ 2u($I$) |
| *f and w scans* | $R_{int} = 0.056$ |
| *Absorption correction: multi-scan SADABS2016/2 (Bruker,2016/2) was used for absorption correction. wR2(int) was 0.0718 before and 0.0565 after correction. The Ratio of minimum to maximum transmission is 0.9424. The l/2 correction factor is Not present.* | $\theta_{max} = 26.0°$, $\theta_{min} = 1.9°$ |
| *Tmin = 0.703, Tmax = 0.745* | $h$ = -17→17 |
| *45300 measured reflections* | $k$ = -17→15 |
| *15041 independent reflections* | $l$ = -23→24 |
| Refinement on $F^2$ | 1456 restraints |
| Least-squares matrix: full | 116 constraints |
| $R[F^2 > 2\sigma(F^2)] = 0.083$ | H-atom parameters constrained |
| $wR(F^2) = 0.194$ | $w = 1/[\sigma^2(F_o^2) + (0.0303P)^2 + 11.0168P]$ where $P = (F_o^2 + 2F_c^2)/3$ |
| $S = 1.09$ | $(\Delta/\sigma)_{max} = -0.0005$ |
| 15041 reflections | $\Delta\rho_{max} = 0.52$ e Å$^{-3}$ |
| 974 parameters | $\Delta\rho_{min} = -0.41$ e Å$^{-3}$ |

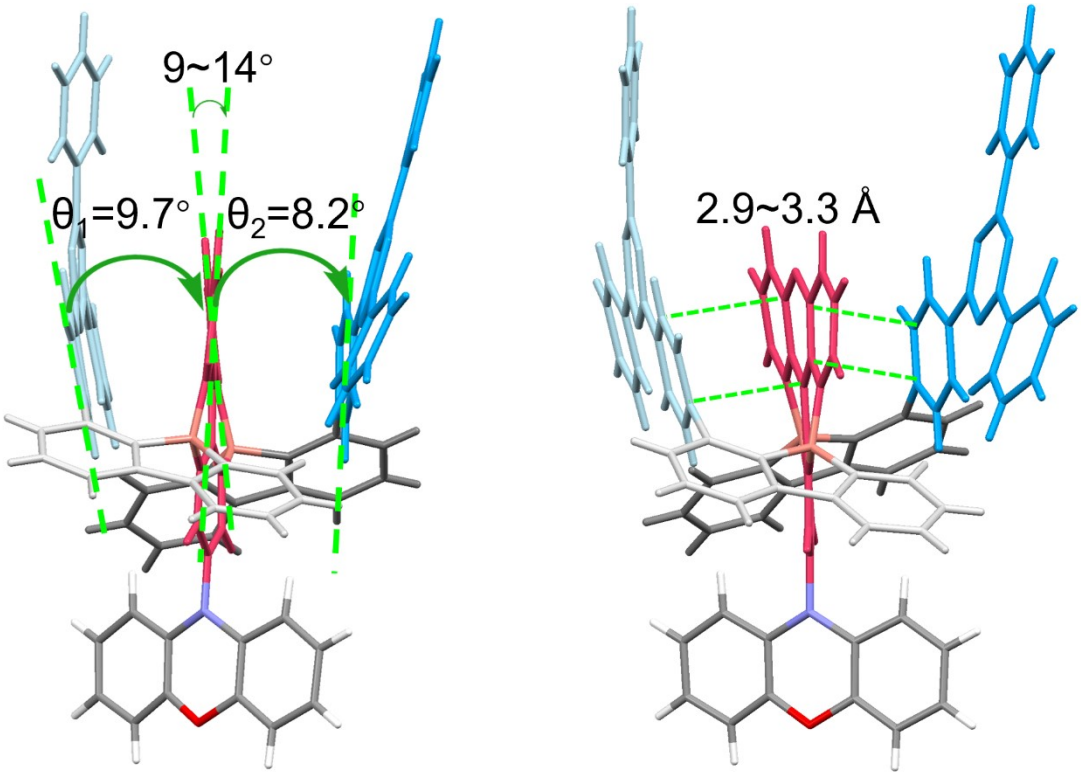


**Figure S7**. Single-crystal structure analysis of **dSFQP**.

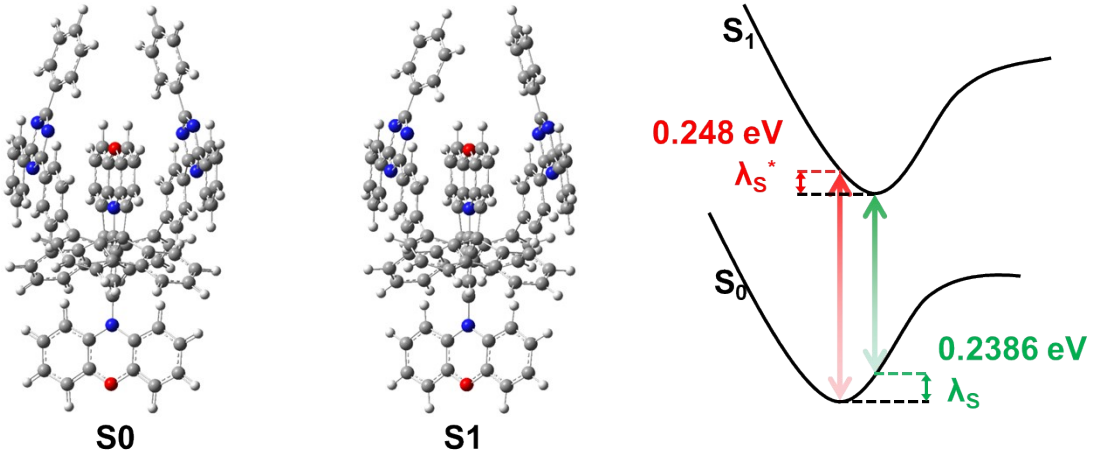


**Figure S8.** a) Optimized ground state configuration and b) optimized excited state configurationfor dSFQP. c) Potential energy surfaces in the ground and the excited states. Reorganization energy=$\lambda_S + \lambda_S^*$.

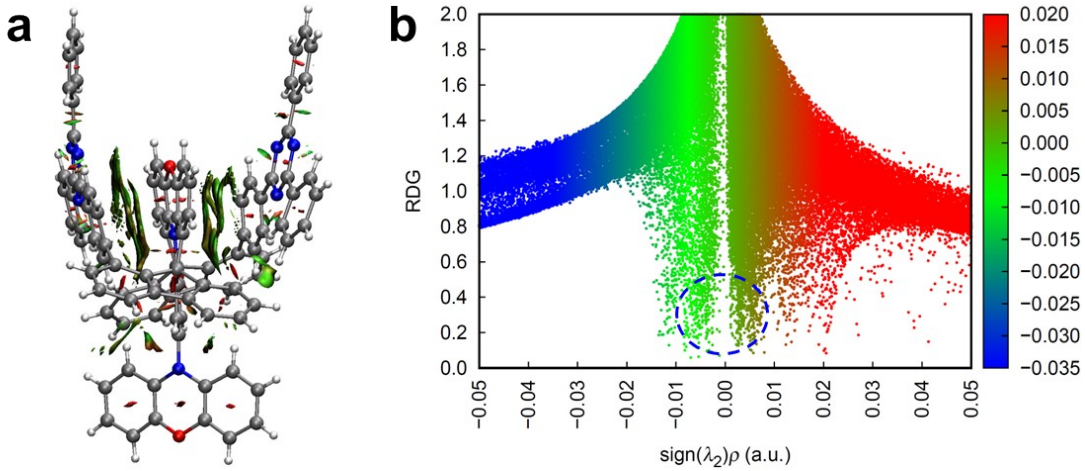


**Figure S9**. The reduced density gradient (RDG) isosurfaces and scattering diagrams of **dSFQP** based on crystal structure.

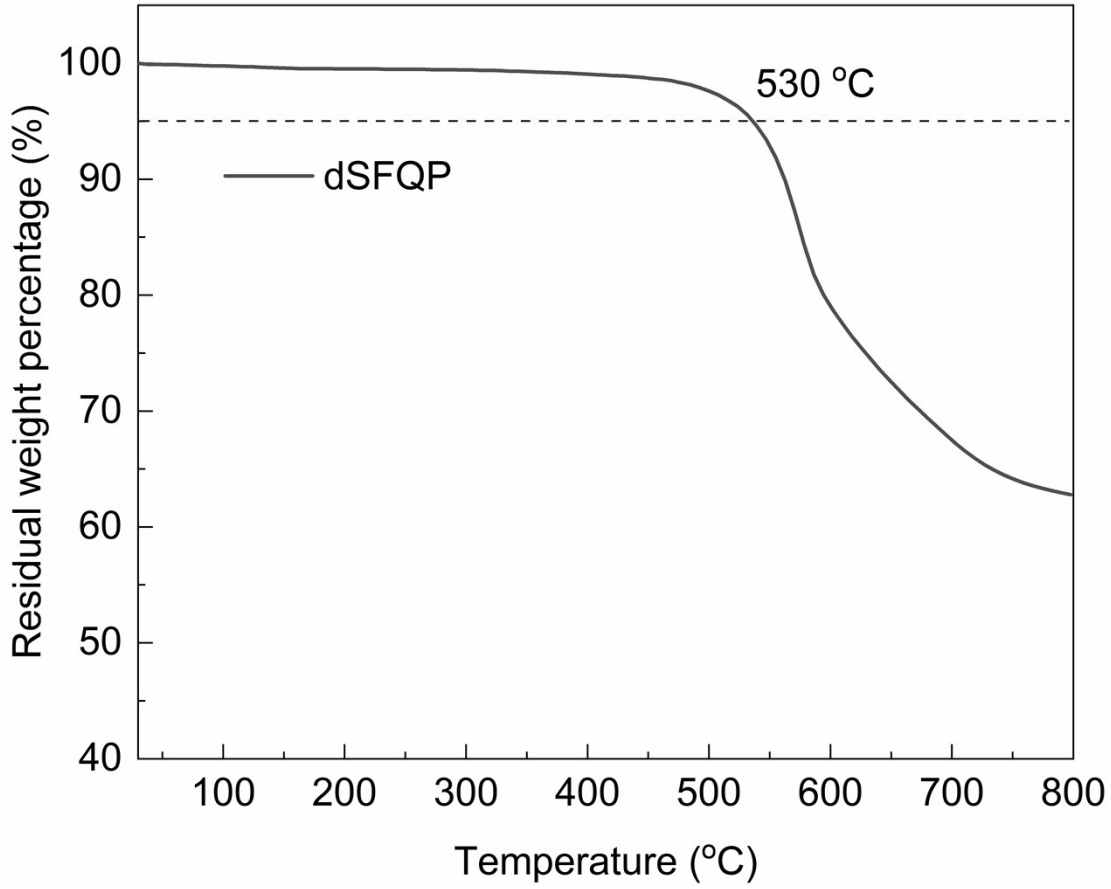


**Figure S10**. TGA curves of **dSFQP**.

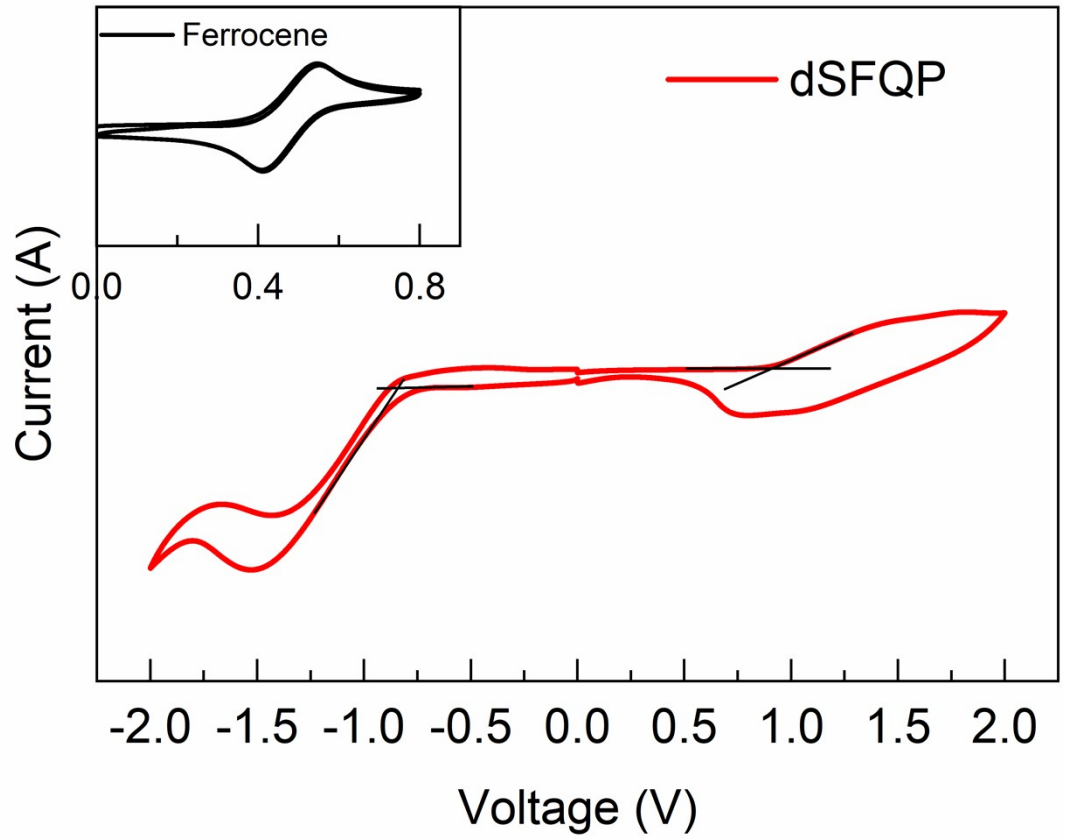


**Figure S11**. Cyclic voltammetry (CV) diagrams of **dSFQP**.

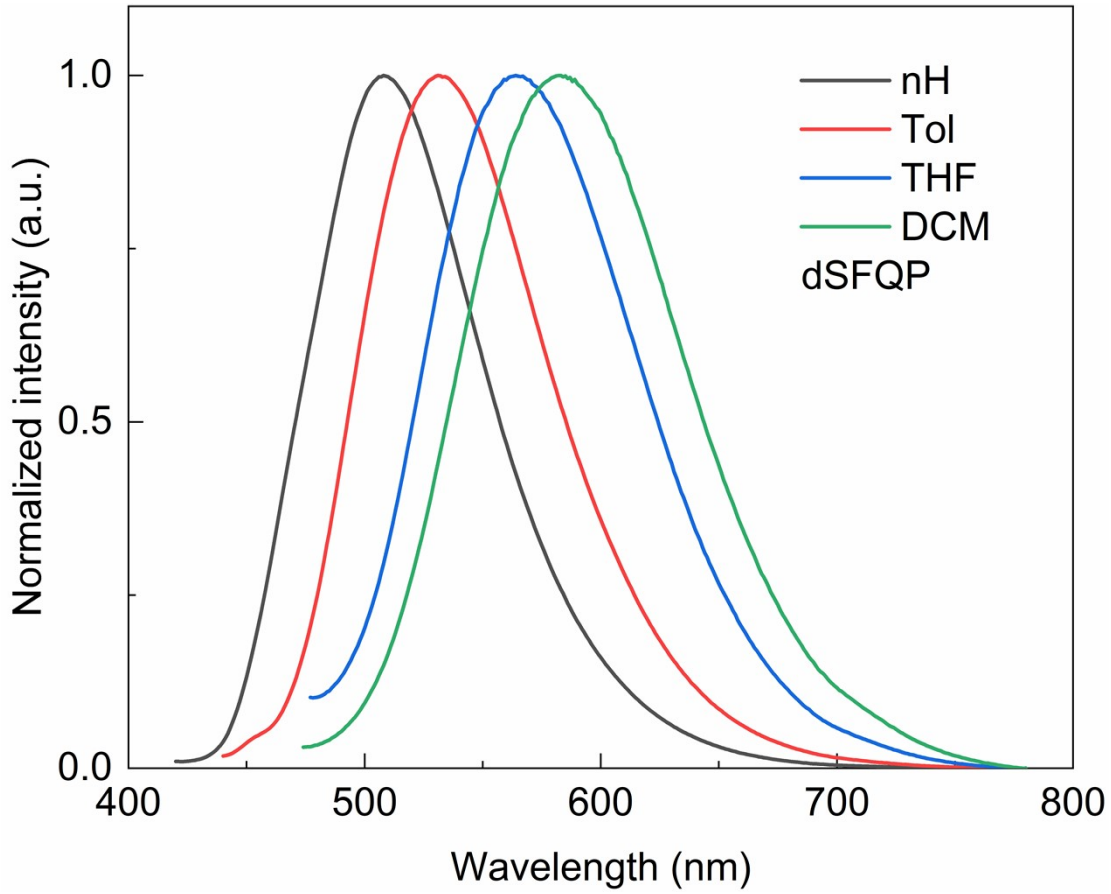


**Figure S12**. PL spectra of **dSFQP** in various solvents (n-H: n-hexane, Tol: toluene, Diox: 1,4-dioxane, THF: tetrahydrofuran, DCM: dichloromethane).

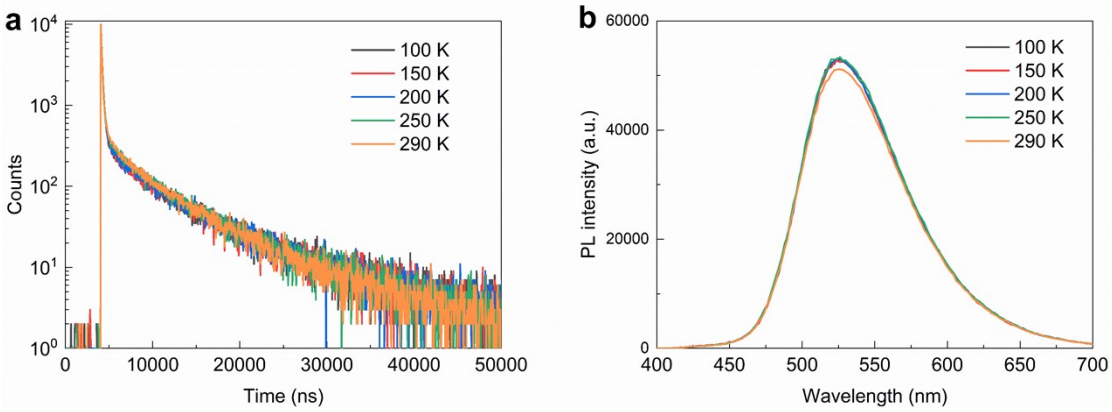


**Figure S13.** Lifetime and spectra of **dSFQP**-doped film as a function of temperature under high vacuum.

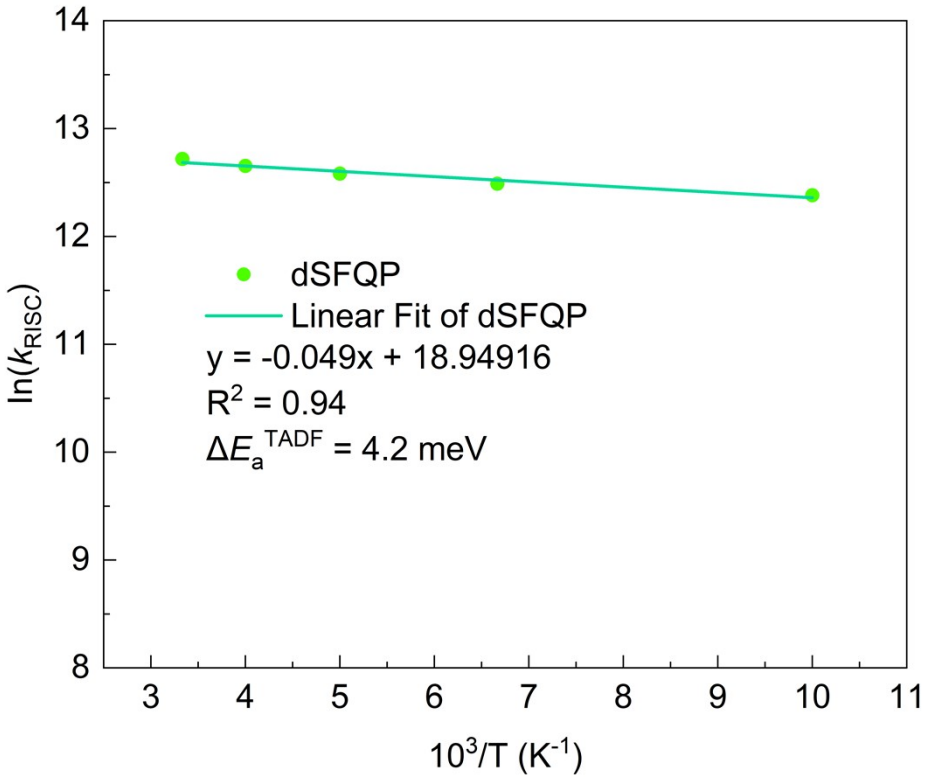


**Figure S14**. Arrhenius plot of the $k_{RISC}$ of **dSFQP** in doped film.

**Table S3.** Photophysical characteristics of **dSFQP** and 2PXZ-2TRZ.

| Films[a] | $\Phi_p$ [%][b] | $\Phi_d$ [%][b] | $\tau_p$ [ns][c] | $\tau_d$ [μs][c] | $k_r$ [$10^6$ $s^{-1}$][d] | $k_{nr}$ [$10^6$ $s^{-1}$][e] | $k_{ISC}$ [$10^6$ $s^{-1}$][f] | $k_{RISC}$ [$10^6$ $s^{-1}$][g] |
|---|---|---|---|---|---|---|---|---|
| 20 wt% **dSFQP** | 32 | 64 | 80 | 3.15 | 4.23 | 0.17 | 8.08 | 0.97 |
| 100wt% **dSFQP** | 13.7 | 24.3 | 35 | 0.5 | 4.40 | 7.18 | 16.99 | 5.95 |
| 2PXZ-2TRZ | 31 | 63 | 107.72 | 5.27 | 2.99 | 0.19 | 6.10 | 0.59 |

[a] 20 wt% **dSFQP** doped in mCBP film, 100 wt% **dSFQP** film and 30 wt% 2PXZ-2TRZ doped in PPF film.

[b] Quantum yields for prompt fluorescence ($\Phi_p$) and delayed fluorescence ($\Phi_d$) for the neat film, $\Phi_p + \Phi_d = \Phi_{PL}$.

[c] Lifetime of the prompt component ($\tau_p$) and delayed component ($\tau_d$) as determined from the transient PL.

[d] Radiative rate constants of $S_1$, $k_r = \Phi_p/\tau_p + \Phi_d/\tau_d$.

[e] Nonradiative rate constants of $S_1$, $k_{nr} = k_r(1 - \Phi_{PL})/\Phi_{PL}$.

[f] Rate constants for ISC ($S_1 \rightarrow T_1$), $k_{ISC} = k_p - k_r - k_{nr}$.

[g] Rate constants for RISC ($T_1 \rightarrow S_1$), $k_{RISC} = k_p k_d / k_{ISC} \cdot \Phi_d/\Phi_p$.

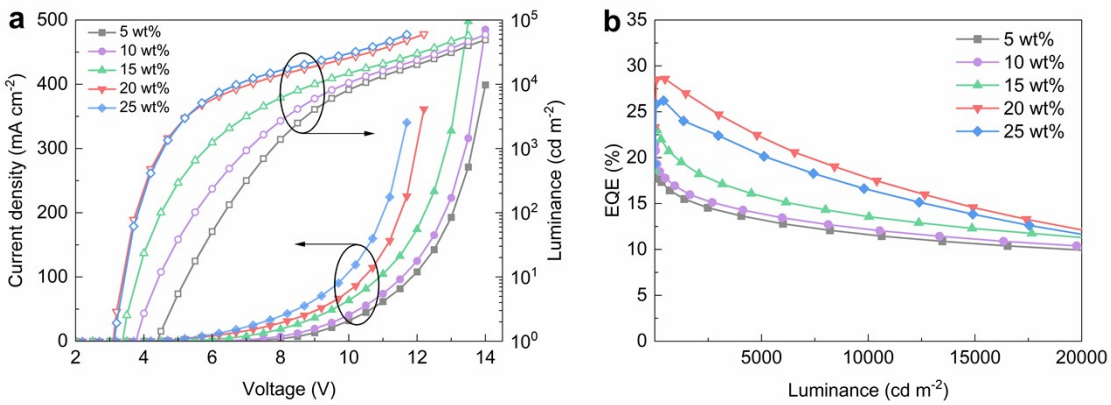


**Figure S15**. a) J-V-L curves and b) EQE versus luminance of devices with different doping concentration.

**Table S4.** Device performance of OLEDs based on **dSFQP** at different doping concentrations.

| EML | $V_{on}$[a] [V] | $L_{max}$[b] [cd $m^{-2}$] | EQE[c] [%] | CE[d] [cd $A^{-1}$] | PE[d] [lm $W^{-1}$] | $\lambda_{EL}$[e] [nm] | CIE[e] (x, y) |
|---|---|---|---|---|---|---|---|
| 5 wt% | 4.5 | 48980 | 19.3/15.8 | 48.7 | 30.2 | 534 | (0.34, 0.55) |
| 10 wt% | 3.9 | 59230 | 21.5/16.9 | 56.5 | 43.4 | 540 | (0.36, 0.55) |
| 15 wt% | 3.5 | 56560 | 23.2/19.6 | 58.6 | 46.0 | 544 | (0.38, 0.55) |
| 20 wt% | 3.2 | 60260 | 28.5/27.7 | 93.3 | 78.8 | 550 | (0.39, 0.55) |
| 25 wt% | 3.2 | 59320 | 26.2/24.6 | 84.9 | 71.0 | 550 | (0.39, 0.55) |
| 100 wt% | 2.8 | 37740 | 10.7/10.3 | 32.8 | 28.5 | 562 | (0.45, 0.53) |

[a] Turn-on voltage. [b] Maximum luminance. [c] EQE at maximum and 1,000 cd $m^{-2}$. [d] Maximum CE and PE. [e] EL peak and CIE coordinates were recorded at 5,000 cd $m^{-2}$.

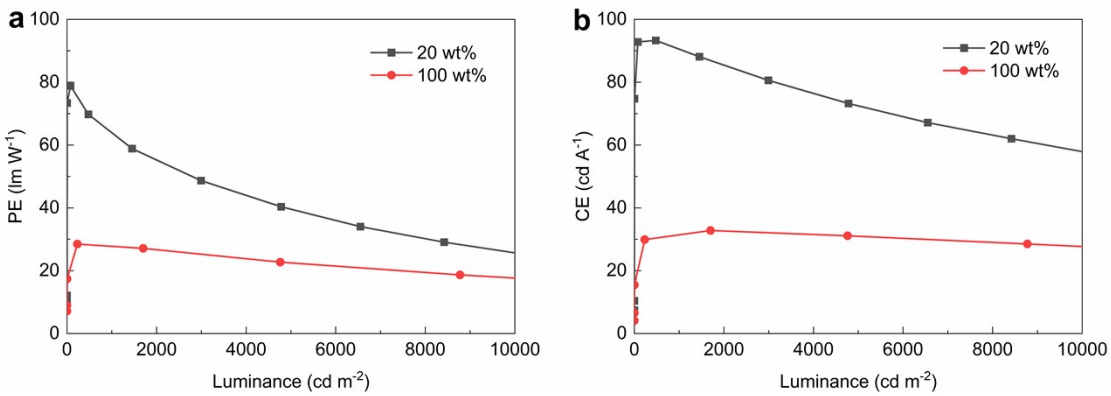


**Figure S16**. PE and CE versus luminance of **dSFQP** with 20 wt% and 100 wt% doping concentrations.

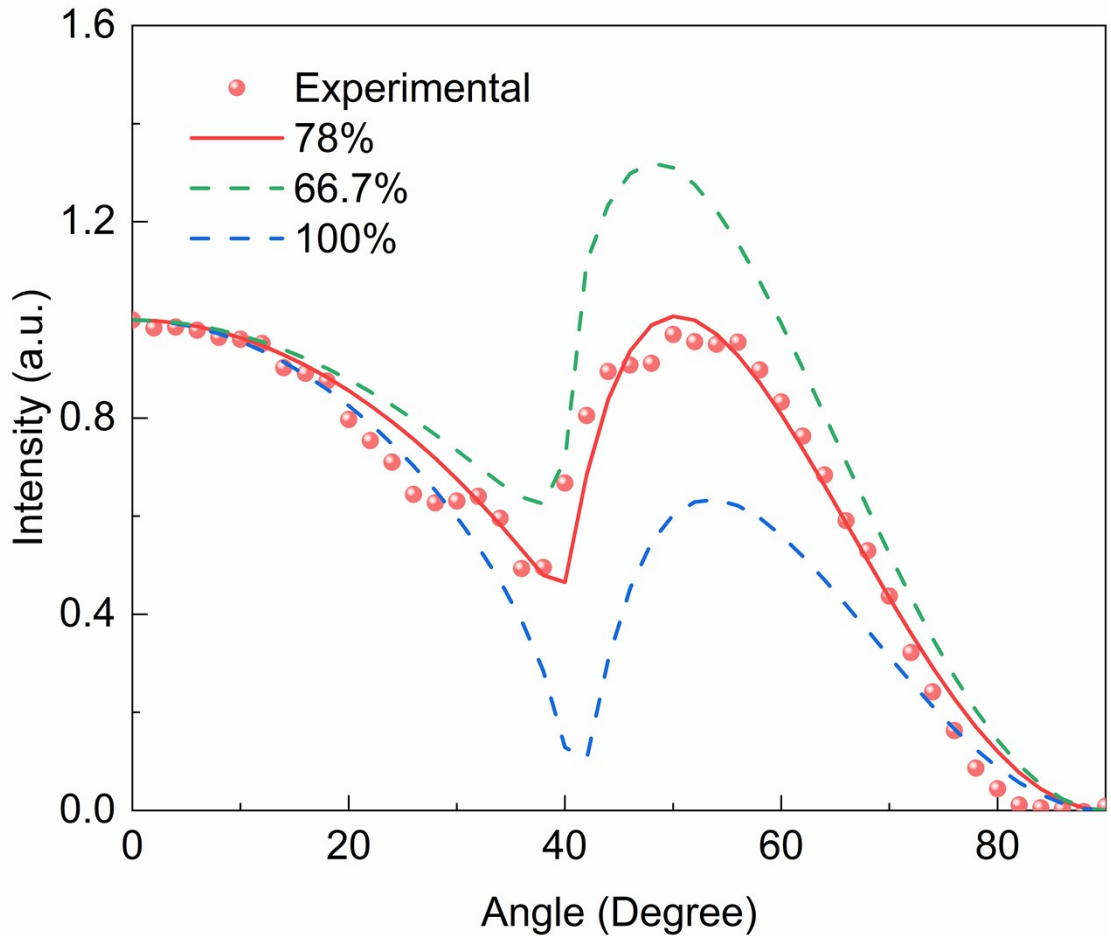


**Figure S17.** Measured horizontal emitting dipole orientation ($\Theta_{//}$) of 20 wt% doped **dSFQP** film.

**Table S5.** OLED performances of the reported TSCT-TADF by vacuum evaporation.

| Emitters | $V_{on}$ [V] | EQE (%) | | | $EQE_{roll-off}$ (%)[b] | $\lambda_{EL}$ [nm] | $L_{max}$ [cd $m^{-2}$] | Ref. |
|---|---|---|---|---|---|---|---|---|
| | | Maximum | 1000 cd $m^{-2}$ | 10000 cd $m^{-2}$ | | | | |
| **dSFQP** | **3.2** | **28.5** | **27.7** | **17.5** | **2.8** | **550** | **60260** | **This work** |
| **dSFQP**[a] | **2.8** | **10.7** | **10.3** | **8.9** | **4.8** | **562** | **37740** | **This work** |
| 2PXZ-2TRZ | 3.0 | 27.1 | 17.7 | 10.4 | 34.7 | 508 | 21620 | [1] |
| 2PXZ-2TRZ[a] | 3.3 | 10.2 | 9.9 | 7.2 | 2.9 | 518 | 26420 | [1] |
| SFST | 3.6 | 12.5 | 11.3 | — | 9.6 | 508 | — | [2] |
| SFOT | 4.0 | 23.1 | 21.3 | — | 7.8 | 508 | — | [2] |
| DM-B | 2.8 | 27.4 | 24.4 | — | 10.9 | 488 | — | [3] |
| DM-Bm | 2.6 | 21.7 | 19.7 | — | 9.2 | 500 | — | [3] |
| DM-G | 3.0 | 18.5 | 15.4 | — | 16.8 | 500 | — | [3] |
| DM-X | 3.4 | 4.3 | — | — | — | 500 | — | [3] |
| STF-DPS | 3.8 | 2.1 | — | — | — | 468 | — | [4] |
| STF-DBTS | 4.0 | 10.3 | — | — | — | 488 | — | [4] |
| DM-BD1 | 3.1 | 28.0 | 22.7 | — | 18.9 | — | — | [5] |
| DM-BD2 | 3.1 | 26.6 | 22.4 | — | 15.8 | — | — | [5] |
| SDMAC | 3.4 | 28.4 | 17.1 | — | 39.8 | 492 | 5997 | [6] |
| Spiro-2P-BT-TPA | 3.3 | 6.6 | 3.0 | — | 54.5 | 520 | — | [7] |
| SAT-DAC | 3.2 | 22.6 | 18.4 | 7.4 | 19.9 | 520 | 9896 | [8] |
| SATX-DAC | 3.5 | 20.9 | 17.0 | 9.5 | 18.6 | 524 | 15540 | [8] |
| 1 | 3.0 | 20.9 | 13.7 | — | 34.4 | 494 | 8600 | [9] |
| 2 | 2.8 | 16.1 | 13.5 | — | 16.1 | 527 | 11000 | [9] |
| 3 | 2.9 | 17.7 | 13.3 | — | 24.8 | 503 | 8800 | [9] |
| 4 | 2.9 | 20.0 | 15.6 | — | 22.0 | 507 | 11000 | [9] |
| 5 | 2.7 | 13.2 | 11.7 | — | 11.4 | 550 | 39000 | [9] |
| SPS | 3.6 | 8.5 | 2.0 | — | 76.5 | 520 | 1678 | [10] |
| SPO | 3.9 | 17.8 | 14.2 | — | 20.2 | 528 | 8260 | [10] |
| SPON | 3.7 | 14.4 | 12.7 | — | 11.8 | 552 | 8808 | [10] |
| TRZ-STFMe | 2.8 | 29.6 | 26.5 | — | 10.4 | 500 | 22940 | [11] |
| TRZ-STFPh | 3.2 | 23.1 | 13.3 | — | 42.4 | 494 | 7280 | [11] |
| DPXZ-QX | — | 20.56 | 5.43 | — | 73.6 | 597 | 15400 | [12] |
| DPXZ-2QX | — | 23.16 | 14.39 | — | 37.8 | 609 | 28400 | [12] |
| TpAT-tFFO | — | 19.2 | 18.1 | 14.4 | 5.4 | 498 | 33870 | [13] |
| PXZ-CTZ | — | 16.57 | 9.93 | — | 40.1 | — | 14500 | [14] |
| DPXZ-CTZ | — | 19.71 | 9.25 | — | 53.1 | — | 3500 | [14] |
| DPXZ-BO | — | 23.96 | 20.23 | — | 15.6 | — | 24500 | [14] |
| dCz-Xo-TRZ | — | 27.8 | 23.9 | — | 14.0 | 477 | — | [15] |
| mCz-Xo-TRZ | — | 21.0 | 17.0 | — | 19.0 | 464 | — | [15] |
| 2tDMG | — | 30.8 | 28.5 | — | 7.5 | 504 | — | [16] |
| 3tDMG | — | 26.3 | 23.2 | — | 11.8 | 518 | — | [16] |

[a] Neat emitter as EML. [b] Efficiency roll-off at 1000 cd $m^{-2}$.

## References


[1] F. M. Xie, H. Z. Li, K. Zhang, Y. Shen, X. Zhao, Y. Q. Li, J. X. Tang, *Angew. Chem. Int. Ed.* **2022**, *61*(49), e202213823.

[2] S. Yang, Y. Wang, C. Peng, Z. Wu, S. Yuan, Y. Yu, H. Li, T. Wang, H. Li, Y. Zheng, Z. Jiang, L. Liao, *J. Am. Chem. Soc.* **2020**, *142*(41), 17756-17765.

[3] X. Tang, L. Cui, H. Li, A. J. Gillett, F. Auras, Y. Qu, C. Zhong, S. T. E. Jones, Z. Jiang, R. H. Friend, L. Liao, *Nat. Mater.* **2020**, *19*(12), 1332-1338.

[4] S. Y. Yang, Q. S. Tian, Y. J. Yu, S. N. Zou, H. C. Li, A. Khan, Q. H. Wu, Z. Q. Jiang, L. S. Liao, *J. Org. Chem.* **2020**, *85*(16), 10628-10637.

[5] X. Q. Wang, S. Y. Yang, Q. S. Tian, C. Zhong, Y. K. Qu, Y. J. Yu, Z. Q. Jiang, L. S. Liao, *Angew. Chem. Int. Ed.* **2021**, *60*(10), 5213-5219.

[6] S. Y. Yang, Z. Q. Feng, Z. Fu, K. Zhang, S. Chen, Y. J. Yu, B. Zou, K. Wang, L. S. Liao, Z. Q. Jiang, *Angew. Chem. Int. Ed.* **2022**, *61*(34), e202206861.

[7] S. Yang, Y. Zhang, F. Kong, Y. Yu, H. Li, S. Zou, A. Khan, Z. Jiang, L. Liao, *Chem. Eng. J.* **2021**, *418*, 129366.

[8] R. Wang, Z. Li, T. Hu, L. Tian, X. Hu, S. Liu, C. Cao, Z. Zhu, J. Tan, Y. Yi, P. Wang, C. Lee, Y. Wang, *ACS Appl. Mater. Interfaces* **2021**, *13*(41), 49066-49075.

[9] Y. Song, M. Tian, R. Yu, L. He, *ACS Appl. Mater. Interfaces* **2021**, *13*(50), 60269-60278.

[10] J. Liu, Z. Feng, C. Peng, Y. Yu, S. Yang, Z. Jiang, L. Liao, *Chin. Chem. Lett.* **2023**, *34*(6), 107634.

[11] W. Chen, M. Zheng, Y. Wu, R. Wang, J. Jin, S. Chen, B. Liu, J. Chen, Y. Huo, S. Ji, *Chem. Eng. J.* **2024**, ***480***, 148314.

[12] C. Jiang, J. Miao, D. Zhang, Z. Wen, C. Yang, K. Li, *Research* **2022**, *2022*, 9892802.

[13] Y. Wada, H. Nakagawa, S. Matsumoto, Y. Wakisaka, H. Kaji, *Nat. Photonics* **2020**, *14*(10), 643-649.

[14] C. Wu, W. Liu, K. Li, G. Cheng, J. Xiong, T. Teng, C. M. Che, C. Yang, *Angew.*

*Chem. Int. Ed.* **2021**, *60*(8), 3994-3998.

[15] T. Huang, Q. Wang, G. Meng, L. Duan, D. Zhang, *Angew. Chem. Int. Ed.* **2022**, *61*(12), e202200059.

[16] C. C. Peng, S. Y. Yang, H. C. Li, G. H. Xie, L. S. Cui, S. N. Zou, C. Poriel, Z. Q. Jiang, L. S. Liao, *Adv. Mater.* **2020**, *32*(48), 2003885.